Oxidation of tartrazine with ultraviolet light emitting diodes: pH and duty cycles effects

Brandon M. Stewart, Michael E. Miller, David M. Kempisty, John Stubbs and Willie F. Harper, Jr

ABSTRACT

The presence of tartrazine (TAR) in the water cycle poses serious threats to human health. This study investigated the used of light emitting diodes (LEDs) in the advanced oxidation of TAR under different pH and duty cycle (DC) conditions. The first order reaction rate constant for TAR oxidation was positively correlated with DC, negatively correlated with pH, and typically greatest at pH 6. Chemical byproduct analysis indicated that OH addition, H abstraction, and electron transfer without molecule transfer were among the relevant reaction mechanisms for TAR degradation. Six byproducts were identified, four were reported for the first time, and two demonstrated that TAR rings were cleaved. This research is the first to determine the optimal pH for UVLED-driven oxidation of TAR and the first to identify new TAR-related byproducts from UVLED-based water treatment.

Key words | advanced oxidation, reaction mechanisms, tartrazine, ultraviolet light-emitting diodes (UVLED)

Brandon M. Stewart
Michael E. Miller
David M. Kempisty
John Stubbs
Willie F. Harper, Jr (corresponding author)
Environmental Engineering and Science Program,
Department of Systems Engineering and Management,
Air Force Institute of Technology,
2950 Hobson Way, Wright-Patterson AFB,
OH 45433, USA
E-mail: *willie.harper@afit.edu*

INTRODUCTION

Tartrazine (TAR) is the trisodium salt of 3-carboxy-5-hydroxy-1-p-sulfophenyl-4-p-sulfophenylazopyrazole, a synthetic dye containing two aromatic rings conjugated by an azo bond (N = N). The practical uses for TAR are in the manufacture of common drugs, foods, and cosmetics. TAR has now emerged as a water contaminant of concern because of its widespread use, high liquid solubility, and a growing critical body of evidence linking it to a wide range of negative health effects, including mental disorders, migraines, allergies, cancer, and respiratory problems (Thuvander 1995; El-Wahab & Moram 2013). TAR can be partially removed from contaminated water using adsorbents (Baraka 2012; Vargas *et al.* 2012a; Vargas *et al.* 2012b; Weber *et al.* 2014; Srivastava *et al.* 2015), photocatalysis (Rao *et al.* 2017; Sebti *et al.* 2017), or electrocoagulation (Thiam *et al.* 2014), but there is a need to explore other treatment alternatives.

Advanced oxidation processes (AOPs) have the potential to meet this need because they utilize radicals which rapidly and non-selectively oxidize many electron-rich organic pollutants and their byproducts (Crittenden *et al.* 2012; Benjamin & Lawler 2013; Yu *et al.* 2015). AOPs can degrade TAR (Andriantsiferana *et al.* 2014; Oancea & Meltzer 2014; GilPavas *et al.* 2015); however, these studies used UV lamps that are troublesome and hazardous because of the mercury contained in the tubes. A relatively new AOP can now be implemented that uses ultraviolet light-emitting diodes (UVLEDs) in place of mercury lamps. UVLEDs are low-cost, light-weight, robust, nonhazardous devices, and they can be powered by low, direct current voltage, which allows the use of portable power sources such as batteries or photovoltaic cells (Ibrahim 2012; Crystal 2013). UVLED-driven AOPs have been used to degrade soluble organics (Wang *et al.* 2013; Duckworth *et al.* 2015; Eskandarloo *et al.* 2015). Scott *et al.* 2017 also showed that TAR can be partially degraded with low power UVLEDs, but their experiments did not identify byproducts or reaction mechanisms.

The objective of this work was to determine the effect of pH and duty cycle (DC) on the oxidation of TAR. This research determined the first order rate constants and reaction mechanisms that apply to TAR oxidation with a UV/H_2O_2-based AOP that produces hydroxyl radicals with LEDs. DC is the percentage of time that the LED lights are turned on, and it becomes an important operating parameter when the LEDs are periodically left off. This

doi: 10.2166/wst.2018.045

pulsing is used to extend the life of the LED and it is clear that DC is positively correlated with oxidation efficiency (Duckworth *et al.* 2015; Scott *et al.* 2017), but the effect of DC on TAR transformation mechanisms has not yet been elucidated. The pH is well-known to influence a variety of AOPs (Crittenden *et al.* 2012), but this has not been investigated for the oxidation of TAR using LED-based AOPs. In principle, reaction rates are expected to decrease as pH rises above 7 because hydroxyl radicals may react with carbonate species as well as HO_2^-, the dissociated form of H_2O_2 (Crittenden *et al.* 2012). The pH may also impact observed reaction rates by altering the intrinsic reactivity of the pollutant, in some cases (Parr & Yang 1989). There is a need to determine the mechanisms that explain the observed relationships between pH and the TAR oxidation rates. There is also a need to clarify the relative roles of pH and DC on reaction kinetics, which may inform design and operational decisions.

MATERIALS AND METHODS

Experimental overview

TAR was oxidized with a UVLED reactor in the presence of H_2O_2 over a range of pH and DC conditions. Byproducts were determined using HPLC-MS, and first order rate constants were determined using the non-steady state solution for the effluent TAR concentration for a complete-mix reactor with reaction. Linear regression modeling was carried out to determine the relative impact of DC and pH on the observed first order rate constants.

Apparatus

The UVLED reactor included drive electronics to control the DC of the LEDs, a continuous-flow reactor containing 245 nm LEDs, and a pump to provide a continuous flow of water (see Figure A1 in supplementary material, available with the online version of this paper). The influent contained H_2O_2 (30% in water from Fisher Scientific, Pittsburgh, PA), deionized water, and TAR (Fisher Scientific, Pittsburgh, PA) and the solution was open to the atmosphere. Each experiment was conducted with approximately 25 mM H_2O_2 and 0.05 mM TAR. Hydroxyl radicals were produced by exposing the H_2O_2 to UV light inside a cylindrical reactor (height and diameter of 7.62 cm) made of electro-polished 316 L stainless steel. Seven 245 nm LEDs (Sensor Electronic Technology, Incorporated, Columbia, SC) were placed in an end plate of the reactor so that the emitting surfaces of the LEDs were in physical contact with the solution. A MasterFlex Console Drive peristaltic pump (model number 77521–50, Gelsenkirchen, Germany) and PharMed® BPT tubing (inner diameter of 0.8 mm, Valley Forge, PA) were employed to move the solution through the reactor at a rate of 0.7 mL per minute. The reactor was mounted on a Corning Stirrer Table (model PC-210, S/N 220197028704, Corning, Inc. Corning, NY) and mechanically mixed with a magnetic stir bar. The absorbance of the effluent at 430 nm was measured using an Agilent Technologies Cary 60 UV-Vis Spectrophotometer (Santa Clara, California). Oxidation of TAR was not observed during control experiments carried out in the presence of H_2O_2 or constant UV light (data not shown).

The DC was controlled with a laptop running DASYLab (DASYLab, version 12, Stamford, CT). This signal included one of six DCs with a frequency of 9.09 hertz. The DCs included five percent (5.5 milliseconds (ms) on, 104.5 ms off), ten percent (11 ms on, 99 ms off), twenty percent (22 ms on, 78 ms off), thirty percent (33 ms on, 77 ms off), fifty percent (55 ms on, 55 ms off), seventy percent (77 ms on, 33 ms off) and one hundred percent (a constant drive signal). An integrating sphere and spectral radiometer (Labsphere, North Sutton, NH) were used to measure the optical power of the LEDs as a function of DC.

Data analysis

The time-dependent effluent concentration of TAR was derived from a mass balance equation for a complete-mix reactor including a reaction:

$$\frac{C}{C_o} = \frac{\tau k_s e^{-(t(k_s + \frac{1}{\tau}))} + 1}{\tau k_s + 1}. \quad (1)$$

In Equation (1), C_0 is the influent TAR concentration, C is the effluent TAR concentration, τ is the average fluid residence time, and k_s is the apparent first order reaction rate constant. This equation was then used to determine k_s using data from experiments. Best-fits were determined using the Microsoft Excel Solver.

Linear regression modeling

Linear regression modeling was carried out to determine the relative roles of pH and DC on the first order rate constants. Briefly, numerous predictor variables were identified and

used in the development of preliminary regression models, and after each model was generated, residuals, studentized residuals, Cook's D Influence, and the square of the model residuals were determined. Valid regression models require normally distributed residuals, constant variance, and independence. The Shapiro-Wilks Test (W-Test) was used to determine whether the residuals were normally distributed, the Breusch-Pagan test was used to confirm constant variance, and the Durbin-Watson test was used to determine that the data sets were independent. Outliers and overly influential points were investigated with histograms of the studentized residuals (no point fell outside ±3 standard deviations) and the overlay plot of Cook's D Influence (no points rank higher than 0.5).

Models that passed the above-referenced tests were evaluated for functionality using the Variance Inflation Factor (scores had to be less than 2 for all parameters). The general formula for the linear regression model is shown in Equation (2):

$$Y = e + \sum_{i=1}^{n} \beta_i X_i \quad (2)$$

where Y is the model's predicted value, e is the intercept, X_i are the predictor variables, and β_i are the regression coefficients. The relative contribution of pH and DC is determined from the sum of the standardized coefficients associated with each predictor variable respectively.

Byproduct analysis

Byproducts were determined by analysis of mass spectra generated by HPLC/MS (Agilent 6130, Santa Clara, CA) with UV detector. The method used a SUPELCO Analytical column (Ascentis ® Express C18, Cat#53829-U, 15 cm × 4.6 mm, 2.7 μm) and a particle fragmentor. The mobile phase was a mixture of 50% acetonitrile and 50% water at 0.35 ml/min. The carrier gas was nitrogen at 10 L/min. API-MS ionization was used for detection. The nebulizer pressure was 45 psig and the quad temperature was 100 °C. The mass ranges were for the positive scans in the 100–700 AMU range, and for the negative scans in the 100–550 AMU range. Samples were stored at 2 °C before HPLC analysis.

RESULTS AND DISCUSSION

The effect of pH and DC on the transformation of TAR

Figure 1 shows the effect of DC on the relative concentration of TAR at pH = 6. The x-axis shows time while the y-axis shows the relative concentration (C/C_0). The degree to which TAR was removed depended on the DC. For example, at 100% DC the final relative concentration was 0.76 while at 50% DC the final relative concentration was 0.87. The lower DC removed less TAR as the reaction was limited by the presence of UV energy, which was

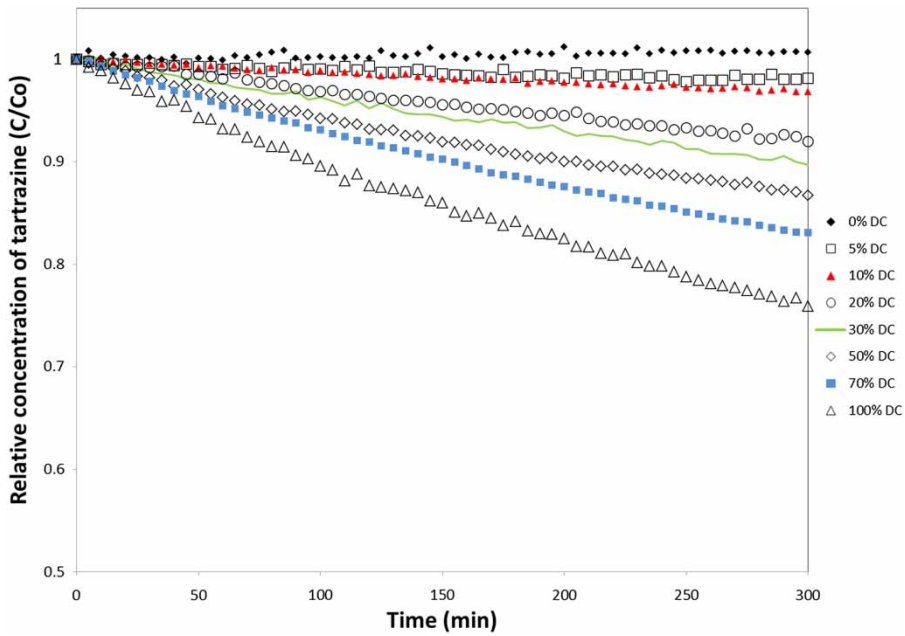

Figure 1 | The effect of DC on the relative concentration of TAR at pH = 6.

reduced by a factor equal to the inverse of the DC. The first order reaction rate constant gradually increased as DC increased. At pH 7, similar results were observed (Figure 2). The extent of TAR oxidation increased gradually as DC was increased from 0% to 100%, with one exception. The reduction in relative concentration for the 50% DC (final relative concentration, C/Co = 0.88) narrowly exceeded the reduction for that of the 70% DC (final relative concentration, C/Co = 0.89). Lower levels of TAR transformation were observed at pH = 8 (Figure A2) and pH = 9 (Figure A3) (Figures A2 and A3 are available with the online version of this paper), and surprisingly in both cases, the extent of TAR transformation was highest at 50% DC, not 100% DC. At pH 6 and 7, the first order reaction rate constants generally increased with DC as reported previously (Duckworth *et al.* 2015, Scott *et al.*, in press) (Figure 3) and the greatest TAR transformation was observed at 100% DC and at pH = 6.

The physical chemistry of TAR does not explain the pH trend noted above. For example, at slightly acidic pH the sodium atoms in TAR are substituted by H atoms to form protonated TAR (pTAR), which is more electrophilic and chemically stable (Mendoza-Huizar 2014). This finding is inconsistent with the results noted above, because TAR was most quickly oxidized at pH 6. There are also no significant differences in the electron density distribution of pTAR and TAR (Mendoza-Huizar 2014). The relative reactivity of pTAR and TAR does not explain the effect of pH on the observed first order rate constants. The measured data showed that increasing the pH negatively impacted TAR oxidation, but the computational data showed that increasing pH did not increase TAR reactivity. The most plausible explanation for the pH trend observed in the current research is that hydroxyl radicals were scavenged by bicarbonate ions, as suggested previously (Buxton *et al.* 1988). This distinction implies that similar pH trends could be observed for the oxidation of other molecules.

Regression model

Multiple linear regression modeling was conducted using binary discrete dependent variables pH and DC to determine model-predicted first order reaction rate constants, and the relative contribution of pH and DC on observed kinetics. The resulting model upheld the three key assumptions for linear regression models: independence (Durbin Watson Test), normally distributed residuals (Shapiro-Wilks Test), and constant variance (Breusch-Pagan Test) (data not shown). The model is presented in Table 1. The regression coefficient with the greatest value was β_9, associated with the 100% DC and pH = 6.

Figure 4 shows the model predicted output plotted with the experimentally determined first order reaction rate constants. The model predicted k values were generally in good agreement with measured k values (adjusted $R^2 = 0.85$). The model's mean predictive error was 7.9×10^{-5} min^{-1}.

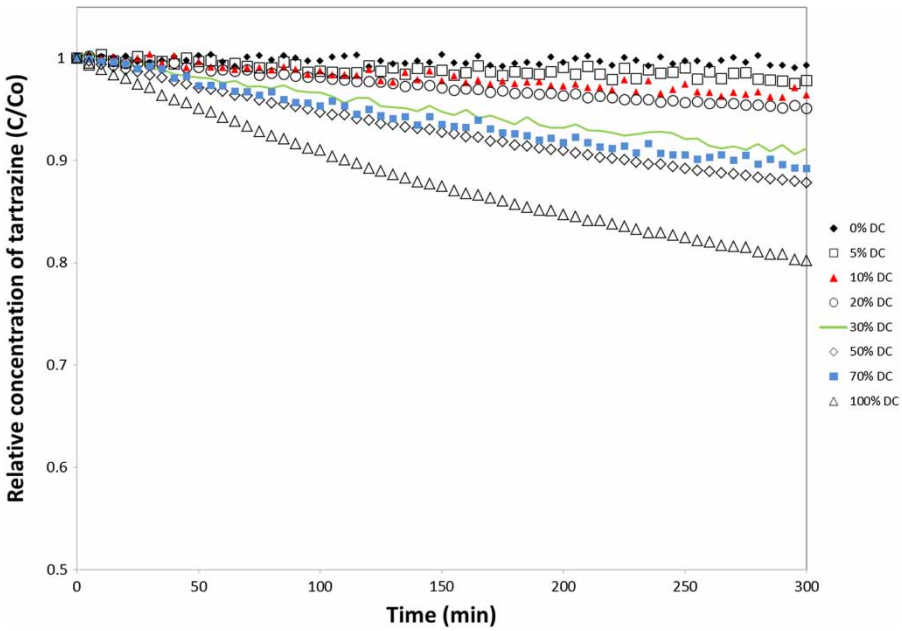

Figure 2 | The effect of DC on the relative concentration of TAR at pH = 7.

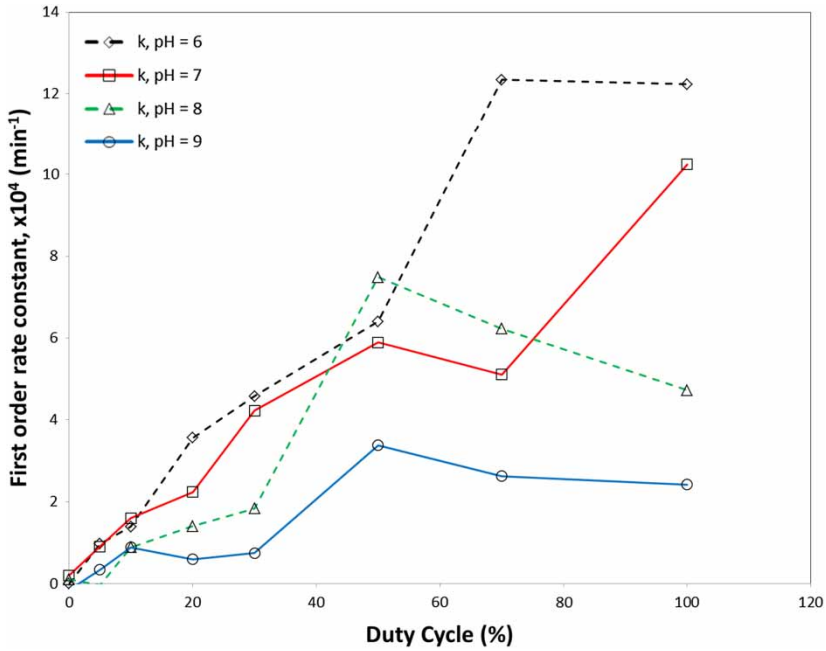

Figure 3 | The effect of pH and DC on the first order rate constant.

Table 1 | Multiple linear regression model $Y = e + \sum_{i=1}^{n} \beta_i X_i$

Constant, $e = 7.9 \times 10^{-5}$

Factors*	Regression coefficients		Discrete variables	
	β_i	Value	X_i	Value
pH 6	β_1	2.6×10^{-4}	X_1	0 or 1
pH 7	β_2	8.9×10^{-5}	X_2	0 or 1
pH 9	β_3	-1.7×10^{-4}	X_3	0 or 1
30% DC	β_4	1.6×10^{-4}	X_4	0 or 1
50% DC	β_5	3.8×10^{-4}	X_5	0 or 1
70% DC	β_6	4.7×10^{-4}	X_6	0 or 1
100% DC	β_7	6.1×10^{-4}	X_7	0 or 1
pH 6 + DC 70	β_8	4.4×10^{-4}	X_8**, α_a, α_b	α_a, $\alpha_b = 0$ or 1
pH 6 + DC 100	β_9	6.8×10^{-4}	X_9**, κ_a, κ_b	κ_a, $\kappa_b = 0$ or 1
pH 7 + DC 100	β_{10}	5.7×10^{-4}	X_{10}**, λ_a, λ_b	λ_a, $\lambda_b = 0$ or 1

*Factors with two terms account for interactions between the experimental conditions.
**X_8, X_9, and X_{10} were defined as follows:.
$X_8 = (\alpha_a - 0.24242)(\alpha_b - 0.18182)$.
$X_9 = (\kappa_a - 0.24242)(\kappa_b - 0.15152)$.
$X_{10} = (\lambda_a - 0.24242)(\lambda_b - 0.15152)$.

The relative contribution of pH and DC is shown in Figure 5. As explained in the methods section, the relative contributions are determined using the standardized coefficients, a metric that explains the contribution that each variable makes to the model output. The relative contribution of the DC (57%) is greater than that of pH (19%); however, there is a notable contribution that is made by the interaction between pH and DC (24%). Table 1 captures this interaction with regression coefficients β_8, β_9, and β_{10}. The implication of this is noteworthy. When pH and DC are simultaneously adjusted to the β_8, β_9, or β_{10} conditions, the observed kinetics are favorably improved beyond what is expected when only pH or DC is adjusted. Alternatively, the same synergism would be expected from unfavorable adjustments. This is the first report, that the authors are aware of, that demonstrates the synergetic impact of pH and DC on UVLED/H_2O_2 AOP.

Byproducts and reaction mechanisms

The chromatographs associated with all of the experiments mentioned above showed three main peaks under both positive and negative ionization (Table 2). The molecular mass of each structure depended on the number of moles of sodium retained on the parent compound. Table 3 shows proposed byproduct structures, which include four that have not been reported previously. The first was unreacted TAR (Product A), which may be partially ionized in solution. The IUPAC name is (E)-5-oxo-1-(4-sulfonatophenyl)-4-((4-sulfonatophenyl)diazenyl)-4,5-dihydro-1H-pyrazole-3-carboxylate.

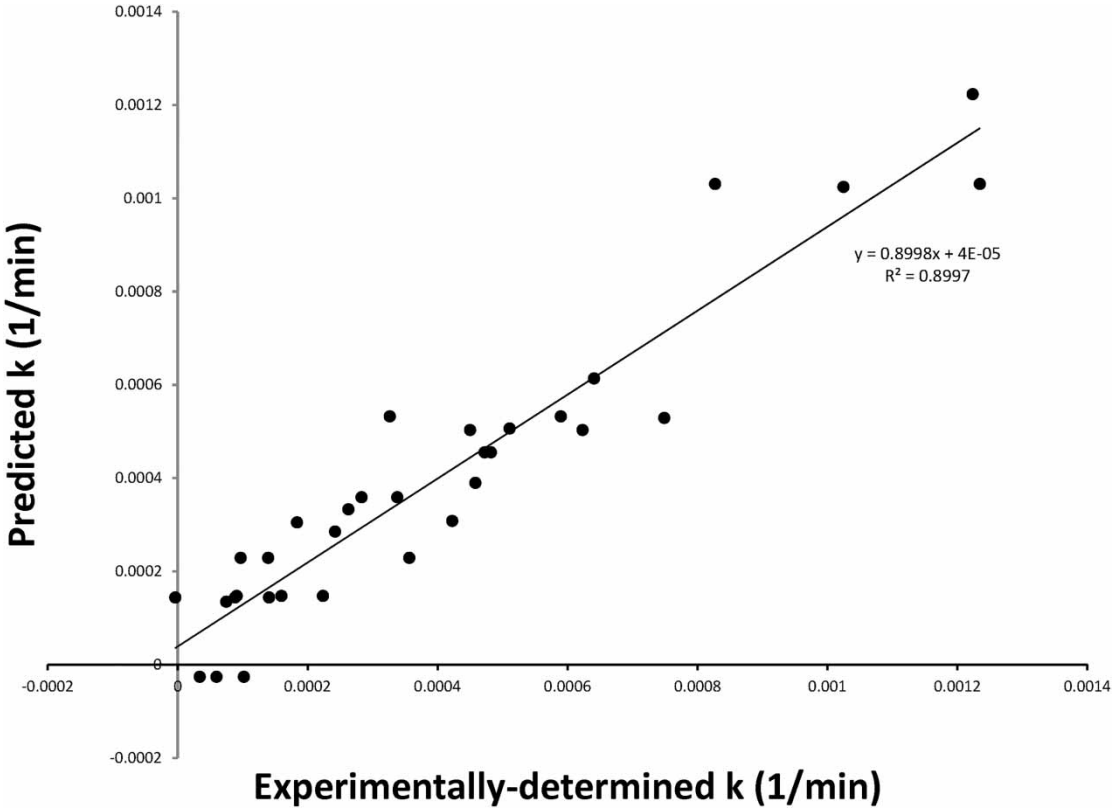

Figure 4 | Experimentally-determined and predicted first order rate constants.

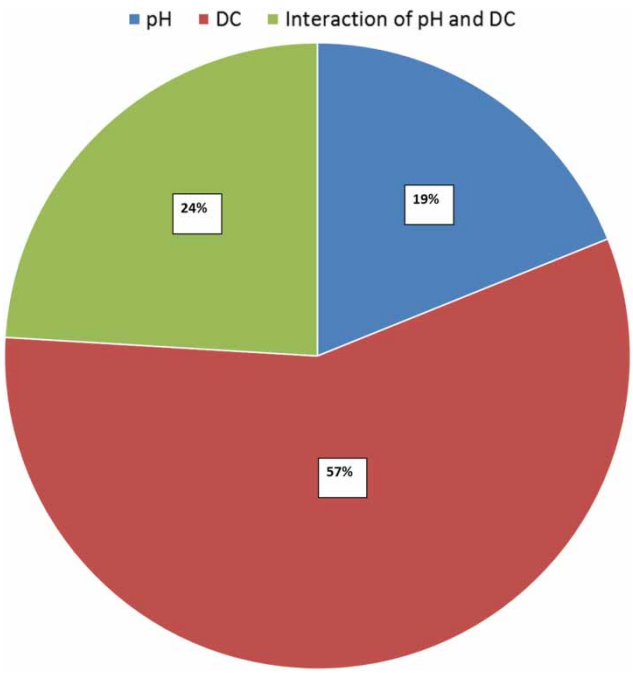

Figure 5 | The relative contribution of pH, DC, and the interaction of pH and DC to first order rate constant.

The second product, denoted Product B, was hydroxylated TAR. The two possible IUPAC names are (E)-4-((2-hydroxy-4-sulfonatophenyl)diazenyl)-5-oxo-1-(4-sulfonatophenyl)-4,5-dihydro-1H-pyrazole-3-carboxylate or (E)-4-(2-hydroxy-2-(4-sulfonatophenyl)-2λ4-diazenyl)-5-oxo-1-(4-sulfonatophenyl)-4,5-dihydro-1H-pyrazole-3-carboxylate. Product C is a reaction byproduct and is similar to a structure reported by dos Santos *et al.* (2014). The IUPAC name for

Table 2 | Proposed byproducts

Retention time	Proposed structure	Ionization	Product name
2.8	Tartrazine (abbrev TAR)	Negative	A
3.3	TAR + OH	Negative	B
3.9	TAR – O – CO_2 + (CN)**	Negative	C
3.1	TAR + 2H	Positive	D
3.6	TAR – sulfonic acid (sulf) – CO_2 + OH + (CN)**	Positive	E
3.9	TAR – sulf + O + (CN)**	Positive	F

**CN from mobile phase and not from AOP reactions.

Table 3 | Proposed byproducts structures by mass, structure, and IUPAC name

Product (Mass*)	Structure	IUPAC name	Reported by others
A (465.39)	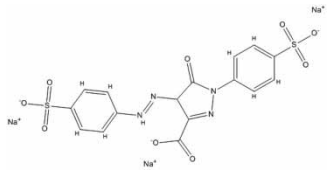	(E)-5-oxo-1-(4-sulfonatophenyl)-4-((4-sulfonatophenyl)diazenyl)-4,5-dihydro-1H-pyrazole-3-carboxylate	Yes[a]
B (482.40)	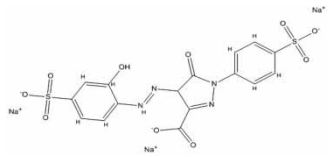	(E)-4-((2-hydroxy-4-sulfonatophenyl)diazenyl)-5-oxo-1-(4-sulfonatophenyl)-4,5-dihydro-1H-pyrazole-3-carboxylate	No[b]
C (405.38)	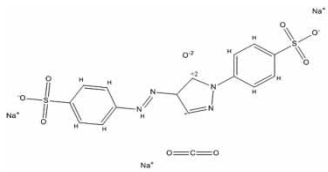	(E)-4-((1-(4-sulfonatophenyl)-4,5-dihydro-1H-pyrazol-4-yl)diazenyl) benzenesulfonate	No[c]
D (467.41)	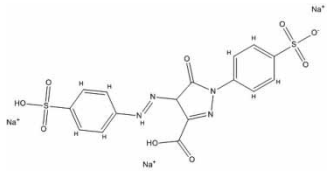	(E)-4-(3-carboxy-5-oxo-4-((4-sulfophenyl)diazenyl)-4,5-dihydro-1H-pyrazol-1-yl)benzenesulfonate or (E)-5-hydroxy-1-(4-sulfonatophenyl)-4-((4-sulfonatophenyl)diazenyl)-4,5-dihydro-1H-pyrazole-3-carboxylate	Yes[d]
E (282.24)	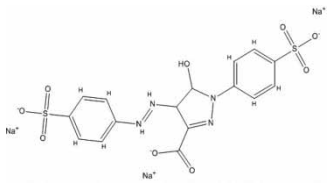	(1-(2-hydroxy-4-sulfonatophenyl)-5-oxo-4,5-dihydro-1H-pyrazol-4-yl) diazen-1-ide	No
F (325.24)	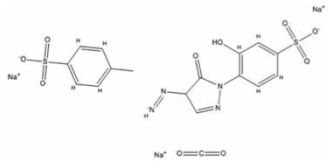	(E)-4-(hydroxydiazenyl)-5-oxo-1-(4-sulfonatophenyl)-4,5-dihydro-1H-pyrazole-3-carboxylate	No

*The mass of sodium is excluded.
[a]Al-Dawery (2013); dos Santos *et al.* (2014); Maslowska & Janiak (1996); Weisz *et al.* (2014).
[b]Similar reaction mechanism discussed by Benjamin & Lawler (2013).
[c]Loss of COO^- Group was demonstrated by dos Santos *et al.* (2014).
[d]dos Santos *et al.* (2014); Maslowska & Janiak (1996).

the proposed structure is (E)-4-((1-(4-sulfonatophenyl)-4,5-dihydro-1H-pyrazol-4-yl)diazenyl)benzenesulfonate.

Product D was either (E)-4-(3-carboxy-5-oxo-4-((4-sulfophenyl)diazenyl)-4,5-dihydro-1H-pyrazol-1-yl)benzenesulfonate or (E)-5-hydroxy-1-(4-sulfonatophenyl)-4-((4-sulfonatophenyl)diazenyl)-4,5-dihydro-1H-pyrazole-3-carboxylate, as previously reported by dos Santos *et al.* (2014) and Maslowska & Janiak (1996), respectively. Both chemicals are likely the result of OH addition followed by the loss of oxygen atoms. Product E is (1-(2-hydroxy-4-sulfonatophenyl)-5-oxo-4,5-dihydro-1H-pyrazol-4-yl)diazen-1-ide, likely the result of OH addition followed (or preceded) by the loss of the sulfonic acid or COO^- group. Electron transfer is indicated by the loss of the sulfonic acid group and the COO^- group. Product F is (E)-4-(hydroxydiazenyl)-5-oxo-1-(4-sulfonatophenyl)-4,5-dihydro-1H-pyrazole-3-carboxylate. The most likely reaction mechanism is hydrogen abstraction followed by an OH addition, the net result of which would be an increase of

one oxygen atom. It is also possible that an oxygen atom (derived from water) was incorporated into the main structure of TAR (before or after loss of the sulfonic acid group).

Concluding remarks

The data collected in the current study is in keeping with the findings of Scott *et al.*, who recently found that TAR is relatively difficult to degrade through the UV/H_2O_2 AOP. Part of the reason for this is the strong absorbance of TAR in the UV spectrum, resulting in nondestructive, radiative transfer and fluorescence (Figure A4, available with the online version of this paper). This mechanism reduces the amount of UV energy available to cleave the O-O bond in H_2O_2 and produce hydroxyl radicals. Therefore, to overcome the absorbance of TAR, more powerful UVLEDs are needed, a finding that we confirmed during follow-up experiments carried out at higher drive current (i.e. 40 mA) levels and with lower (i.e. 0.01 M) influent TAR concentration (Figure A5, available with the online version of this paper). It is also important to note that the likelihood of a UV photon interacting with a TAR or H_2O_2 molecule depends on the molar H_2O_2-to-TAR ratio, which was 500:1 in the current study. In principle, this ratio can impact the production and termination of hydroxyl radicals during the reaction cascade. The kinetics may be limited by inadequate H_2O_2 if the molar H_2O_2-to-TAR ratio is too small or by H_2O_2 quenching (i.e. radicals reacting with H_2O_2) if the ratio is too large. Future studies should explore optimal molar H_2O_2-to-TAR ratios. There are also several reactor design characteristics that impact UV fluence and reaction efficiency, including the hydraulic residence time distribution, the output power, LED wavelength, reactor materials (e.g. Teflon vs. stainless steel), and the arrangement of the LEDs. Future research should seek to optimize these operating factors.

A recent computational study carried out by Mendoza-Huizar 2014 showed that the TAR pyrazole C18 atom, initially bonded to the azo group, has the highest frontier electron density (FED). This computational result, when combined with the structures of the byproducts identified in this study, demonstrates that high FED atoms of TAR (i.e. pyrazole C18) are oxidized by radical attack. This finding bolsters the promise of predicting the TAR degradation pathways *a priori* based on Density Functional Theory, and eventually, determining recalcitrant TAR byproducts that should be further examined for heightened risks to human health. What remains now is to continue to optimize treatment technologies to achieve higher levels of TAR transformation and to identify other byproduct structures and their properties.

CONCLUSIONS

The conclusions of this study are as follows:

1. The first order reaction rate constant for TAR oxidation was statistically and positively correlated with DC, statistically and negatively correlated with pH, and typically greatest at pH 6. DC made a larger impact on the first order rate constant than the pH, but the observed kinetics was also influenced by the interaction of these two variables. Increasing the operating pH in a UVLED reactor decreases TAR degradation by radical scavenging, not by changing the intrinsic reactivity of TAR.
2. Chemical byproduct analysis indicated that OH addition, electron transfer (without molecule transfer), and H abstraction were among the reaction mechanisms for TAR degradation under all experimental conditions. Four new byproduct structures were proposed, including two that demonstrate that TAR rings were cleaved.

ACKNOWLEDGEMENTS

The authors thank Dr Daniel Felker (Chemist, AFIT) for analytical assistance and John Hixenbaugh (Issue Point Manager, AFIT) for assistance with chemical procurement and waste disposal. The authors thank the Defense Environmental Restoration Account for financial support. The authors thank Dr Edward White (AFIT) for assistance with statistical analysis.

DISCLAIMER

The views expressed in this article are those of the authors and do not reflect the official policy or position of the Air Force Institute of Technology, the United States Air Force, the Department of Defense, or the United States government.

REFERENCES

Al-Dawery, S. 2013 Photo-catalyst degradation of tartrazine compound in wastewater using TiO_2 and UV light. *Journal of Engineering Science and Technology* **8** (6), 683–691.

Andriantsiferana, C., Mohamed, E. F. & Delmas, H. 2014 Photocatalytic degradation of an Azo-Dye on TiO_2/Activated carbon composite material. *Environmental Technology* **35** (3), 355–363.

Baraka, A. 2012 Adsorptive removal of tartrazine and methylene blue from wastewater using melamine-formaldehyde-tartaric acid resin (and a discussion about pseudo second order model). *Desalination and Water Treatment* **44** (1–3), 128–141.

Benjamin, M. & Lawler, D. 2013 *Water Quality Engineering: Physical/Chemical Treatment Processes*. John Wiley & Sons, Inc., Hoboken, NJ.

Buxton, G., Greenstock, C., Helman, W. & Ross, A. 1988 Critical review of rate constants for reactions of hydrated electrons, hydrogen atoms and hydroxyl radicals in aqueous solution. *Journal of Physical Chemical Reference Data* **40**, 513–886.

Crittenden, J. C., Trussell, R. R., Hand, D. W., Howe, K. J. & Tchobanoglous, G. 2012 *MWH'S Water Treatment: Principles and Design*. Third Edition, John Wiley & Sons, Inc., Hoboken, NJ.

Crystal, I. S. 2013 *UVC LED Disinfection*. Application Note, Green Island, NY.

dos Santos, T., Zocolo, G., Morales, D., Umbuzeiro, G. & Boldrin Zanoni, M. 2014 Assessment of the breakdown products of solar/UV induced photolytic degradation of food dye tartrazine. *Food and Chemical Toxicology* **68**, 307–315.

Duckworth, K., Spencer, M., Bates, C., Miller, M., Almquist, C., Grimaila, M., Magnuson, M., Willison, S., Phillips, R. & Racz, L. 2015 Advanced oxidation degradation kinetics as a function of ultraviolet LED duty cycle. *Water Science and Technology* **71** (9), 1375–1381.

El-Wahab, H. & Moram, G. S. E. 2013 Toxic effects of some synthetic food colorants and/or flavor additives on male rats. *Toxicology and Industrial Health* **29** (2), 224–232.

Eskandarloo, H., Badiei, A., Behnajady, M. & Ziarani, G. 2015 UV-LEDs assisted preparation of silver deposited TiO_2 catalyst bed inside microchannels as a high efficiency microphotoreactor for cleaning polluted water. *Chemical Engineering Journal* **270**, 158–167.

GilPavas, E., Gomez, C., Rynkowski, J., Dobrosz-Gomez, I. & Gomez-Garcia, M. 2015 Decolorization and mineralization of yellow 5 (E102) by UV/Fe^{2+}/H_2O_2 process. Optimization of the operation conditions by response surface methodology. *Comptes Rendus Chimie* **18** (10), 1152–1160.

Ibrahim, M. A. S. 2012 *Commercial Evaluation of UV-LED in Water Treatment Applications*. *Master's thesis*, School of Applied Sciences, Cranfield University, Cranfield, England.

Maslowska, J. & Janiak, J. 1996 Voltammetric and spectrophotometric studies on tartrazine – a food colorant. *Analytical Chemistry (Warsaw)* **41** (5), 855–864.

Mendoza-Huizar, L. H. 2014 A theoretical study of chemical reactivity of tartrazine through DFT reactivity descriptors. *Journal Mexican Chemical Society* **58** (4), 416–423.

Oancea, P. & Meltzer, V. 2014 Kinetics of tartrazine photodegradation by UV/H2O2 in aqueous solution. *Chemical Papers* **68** (1), 105–111.

Parr, R. G. & Yang, W. 1989 *Density Functional Theory of Atoms and Molecules*. Oxford University Press, New York, NY.

Rao, M. O., Asiri, A. M. & Anandan, S. 2017 Photocatalytic degradation of tartrazine dye using CuO straw-sheaf-like nanostructures. *Water Science and Technology* **75** (6), 1421–1430.

Scott, R., Mudimbi, P., Miller, M. E., Magnuson, M., Willison, S., Phillips, R. & Harper Jr, W. F. 2017 Advanced oxidation of tartrazine and brilliant blue with pulsed ultraviolet light emitting diodes. *Water Environment Research* **89**, 24–31.

Sebti, A., Souahi, F., Mohellebi, F. & Igoud, S. 2017 Experimental study and artificial neural network modeling of tartrazine removal by photocatalytic process under solar light. *Water Science and Technology* **76** (2), 311–322.

Srivastava, V., Maydannik, P., Sharma, Y. C. & Sillanpaa, M. 2015 Synthesis and application of polypyrrole coated tenorite nanoparticles (PPy@TN) for the removal of the anionic food dye 'tartrazine' and divalent metallic ions viz. Pb(II), Cd(II), Zn(II), Co(II), Mn(II) from synthetic wastewater. *RSC Advances* **5** (98), 80829–80843.

Thiam, A., Zhou, M., Brillas, E. & Sires, I. 2014 Two-step mineralization of tartrazine solutions: study of parameters and by-products during the coupling of electrocoagulation with electrochemical advanced oxidation processes. *Applied Catalysis B-Environmental* **150**, 116–125.

Thuvander, A. 1995 Hypersensitivity to azo coloring agents: tartrazine in food may cause rash and asthma. *Lakartidningen* **92** (4), 296–298.

Vargas, A., Cazetta, A., Martins, A., Moraes, J., Garcia, E., Gauze, G., Costa, W. & Almeida, V. 2012a Kinetic and equilibrium studies: adsorption of food dyes Acid Yellow 6, Acid Yellow 23, and Acid Red 18 on activated carbon from flamboyant pods. *Chemical Engineering Journal* **181**, 243–250.

Vargas, A., Martins, A. & Almeida, V. 2012b Ternary adsorption of acid dyes onto activated carbon from flamboyant pods (Delonix regia): analysis by derivative spectrophotometry and response surface methodology. *Chemical Engineering Journal* **195**, 173–179.

Wang, P., Fane, A. & Lim, T. 2013 Evaluation of a submerged membrane vis-LED photoreactor (sMPR) for carbamazepine degradation and TiO_2 separation. *Chemical Engineering Journal* **215**, 240–251.

Weber, C. T., Collazzo, G. C., Mazutti, M. A., Foletto, E. L. & Dotto, G. L. 2014 Removal of hazardous pharmaceutical dyes by adsorption onto papaya seeds. *Water Science and Technology* **70** (1), 102–107.

Weisz, A., Ridge, C., Roque, J., Mazzola, E. & Ito, Y. 2014 Preparative separation of two subsidiary colors of FD&C Yellow No. 5 (Tartrazine) using spiral high-speed countercurrent chromatography. *Journal of Chromatography A* **1343**, 91–100.

Yu, X., Zhou, M., Ren, G. & Ma, L. 2015 A novel dual gas diffusion electrodes system for efficient hydrogen peroxide generation used in electro-Fenton. *Chemical Engineering Journal* **263**, 92–100.

First received 4 December 2017; accepted in revised form 19 January 2018. Available online 6 February 2018